J Membrane Biol (2008) 225:27–37
DOI 10.1007/s00232-008-9130-8

Characterization of the Mechanism of the *Staphylococcus aureus* Cell Envelope by Bacitracin and Bacitracin-Metal Ions

Zu-De Qi · Yi Lin · Bo Zhou · Xiao-Di Ren · Dai-Wen Pang · Yi Liu

Received: 27 May 2008 / Accepted: 11 September 2008 / Published online: 15 October 2008

Abstract Bacitracin is a metal-dependent dodecapeptide antipeptide produced by *Bacillus* species. Microcalorimetry was used to study the antimicrobial activity of bacitracin and bacitracin–metal ion complexation inhibited on *Staphylococcus aureus* at 37°C. The affinity of metal ions binding to bacitracin was investigated by isothermal titration calorimetry and was as follows: Cu(II) ≥ Ni(II) > Co(II) > Zn(II) ≥ Mn(II). The metal ion binding affinity is not relative to the antimicrobial activity of bacitracin–metal complexation. Atomic force microscopic images revealed that the surface of *S. aureus* treated by bacitracin–Zn(II) was rather rough compared to that treated by bacitracin only. The central cell surface displayed small depressed grooves around the septal annulus at the onset of division. Bacitracin mainly inhibited the splitting system within the thick cross walls as seen by transmission electron microscopy (TEM). The inhibition mechanism of bacitracin may be relative to the assistance of Zn(II) coordination with the cell surface as seen by TEM. We can put forward that the activity of bacitracin only inhibited growth and division initially from the synthesis of the cell wall, especially the cell wall of the septal annulus. The divalent metal ions function to increase the adsorption of bacitracin onto the cell surface.

Keywords *Staphylococcus aureus* · Microcalorimetry · Isothermal titration calorimetry · Atomic force microscopy · Thin-section transmission electron microscopy · Bacitracin

Z.-D. Qi · Y. Lin · B. Zhou · X.-D. Ren · D.-W. Pang · Y. Liu (✉)
College of Chemistry and Molecular Sciences,
Wuhan University, Wuhan 430072, People's Republic of China
e-mail: prof.liuyi@263.net

Z.-D. Qi
e-mail: qizude0930@163.com

Z.-D. Qi · Y. Lin · B. Zhou · D.-W. Pang · Y. Liu
State Key Laboratory of Virology, Wuhan University,
Wuhan 430072, People's Republic of China

Y. Liu
College of Chemistry and Environmental Engineering,
Yangtze University, Jinzhou 434020,
People's Republic of China

Introduction

Bacitracin, a metal-dependent dodecapeptide produced by *Bacillus subtilis* and *Bacillus licheniformis* (Toscano and Storm 1982), was first discovered in 1943 from a bacterial culture isolated from a wound of a 7-year-old American girl (Ming and Epperson 2002). Commercial bacitracin preparations are comprised of a mixture of many closely related analogues, named bacitracin A–I, of which bacitracin A represents the major component with the highest activity (Konigsberg and Craig 1962; Hirotsu et al. 1978). It is also known that bacitracins A and B account for 95% of the biological activity of the mixtures (Tsuji and Robertson 1975). Bacitracin A, a dodecapeptide, contains a heptapeptide cyclic structure and a thiazoline ring formed between the L-cysteine and L-isoleucine located at the N-terminal end of the acylic peptide side chain (Konz et al. 1997). Bacitracin has activity primarily against gram-positive cocci and bacilli, including *Staphylococcus*, *Streptococcus* and *Clostridium difficile*, as well as some archaea such as *Methanobacterium*, *Mathanococcus* and *Halococcus* (Storm 1974). It has a medical application in the treatment of gastrointestinal infections, such as antibiotic-associated colitis and diarrhea caused by *C.difficile*

(Chang et al. 1980). It is widely utilized as an animal feed supplement to improve animal body weight and to prevent diseases in agriculture (Nagaraja and Chengappa 1998; Abdulrahim et al. 1999). Consequently, bacitracin is important to the pharmaceutical and livestock industries throughout the world.

The mode of bacitracin action entails forming a complex with the lipid C_{55}-isoprenyl pyrophosphate (IPP), which is mediated by divalent metal ions. This trapping of IPP prevents the dephosphorylation of IPP and therefore interrupts the synthesis of cell walls (Stone and Strominger 1971). Divalent metal ions such as Co(II), Mn (II), Zn(II) and Cu(II) are essential for the antimicrobial activity of bacitracin (Sin et al. 2005; Froyshov 1984). Although bacterial resistance toward virtually all antibiotics on the market has become a threatening health issue in recent years (Monroe and Polk 2000), bacterial resistance toward bacitracin is still limited despite its wide use in the past several decades (Podlesek et al. 1995; Harel et al. 1999). Thus, it can serve as a potential lead for the design of potent antibiotic metallopeptides and analogues, with limited potential to evoke bacterial resistance for combating bacterial infection.

Microbial cell envelopes, which form part of the boundary between the external and the intracellular environment, have several important functions, such as determining cell shape, growth and division; enabling cells to resist turgor pressure; acting as molecular sieves; and mediating molecular recognition and cellular interactions (Touhami et al. 2006). An important component of microbial surface structures is formed by extracellular polymeric substances, such as peptidoglycan, *O*-acetylation and teichoic acid, which plays a critical role in collective motility (Rogers et al. 1980). Atomic force microscopy (AFM) has provided new opportunities for viewing and manipulating microbial surfaces in their native environments (Dufrêne 2004a, b). AFM visualization is accomplished by measuring the interacting repulsive or attractive forces between the tip and the surface of the specimen of a very small, sharp-tipped probe located at the free end of a cantilever (Braga and Ricci 1998, 2000, 2002). Several AFM experiments were carried out to directly observe the morphological alterations of targeting bacterial cells when exposed to antibiotics. Chaw et al. (2005) showed the potential of AFM as a tool to measure the intermolecular forces in biofilm structures and to study the effect of silver ions on sessile *Staphylococcus epidermidis* cell viability and stability. Braga et al. (1997) also investigated the exposure of *Staphylococcus aureus* and *Escherichia coli* strains to cefodizime, cefotaxime and ceftriaxone with AFM and discovered that the mechanism of the three cephalosporins differed between *S. aureus* and *E coli*. Braga and Ricci (2002) showed with the aid of AFM that erythromycin A (a 14-membered ring) and rokitamycin (a 16-membered ring) differed in the manner in which the morphology of *Streptococcus pyogenes* (M phenotype) was influenced.

Although bacitracin inhibition of bacteria has been investigated from the molecular aspect (Storm and Strominger 1973), the precise constant and stoichiometry of the mixture of bacitracin binding to divalent transition ions have not been reported and the effects on cell envelopes and division have not been visually assessed by AFM and transmission electron microscopy (TEM). In this work, microcalorimetry was employed to assess the improvement of Zn(II), Mn(II), Cu(II), Ni(II) and Co(II) on the antimicrobial activity of bacitracin. The method of isothermal titration calorimetry (ITC) was used to investigate the affinity of divalent transition ions with bacitracin without separated bacitracin mixture. We also utilized AFM complemented with thin-section TEM to investigate the changes in the *S. aureus* cell wall before and after treatment by bacitracin, bacitracin–Zn(II) complexation and Zn(II), which was just a model to explain the mechanism of metal ions participating in the antimicrobial activity of bacitracin. These studies can provide a more comprehensive understanding of bacitracin effects on gram-positive bacteria.

Materials and Methods

Bacterial Cultures

S. aureus (CCTCC AB910393), used as target bacterium to investigate the biological activity of bacitracin, was supplied by the China Center for Type Culture Collection of Wuhan University (Wuhan, P.R. China). *S. aureus* was cultured using standard procedures in Luria-Bertani (LB) broth. Cells were harvested by centrifugation, washed three times with deionized water and resuspended to a concentration of 10^8 ml^{-1}.

Microcalorimetric Studies of Bacitracin Inhibition of *S. aureus* Growth

The LKB 2277 Bioactivity Monitor (Thermometric, Jarfalla, Sweden) was used to measure *S. aureus* metabolism in the presence and absence of bacitracin (>99%; Sino-American Biotechnology, Shanghai, China), bacitracin–metal ion complexation and metal ions. The baseline stability of the instrument was $\pm$ 0.2 μW/24 h. The flow-stop microcalorimetric method, according to Suurkuusk and Wadso (1982) and Xie et al. (1988), was utilized. Briefly, the cell suspension containing *S. aureus* (1×10^6 CFU) and appropriate inhibitors (bacitracin, bacitracin-Zn[II] mixture and Zn[II] solutions) was pumped into the flow cell by the aid of an LKB-2132 pump at a flow rate of

50 ml h^{-1}. When the flow-measuring cell of the instrument was full, the pump was stopped and the thermogenic curves, correlating with *S. aureus* metabolism (heat production) at 37°C, were electronically recorded.

ITC Study

All titration experiments were conducted using an ITC instrument (VP-ITC; MicroCal, Northampton, MA, USA). In a typical experiment, bacitracin solution (3 mM) was placed in the 1.413 cm^3 sample cell of the calorimeter and divalent transition ion solutions were loaded into the injection syringe. These concentrations were chosen to obtain a complete binding isotherm, which requires the concentration in the injection syringe to be approximately 10 times the concentration of binding sites in the cell. The bacitracin solution and the divalent transition ion solutions, prepared in acetic acid/sodium acetate buffer (pH 5.0), were degassed for 5 min under vacuum with a Thermo-Vac accessory (MicroCal) prior to performing an experiment. Typically, 10-µl injections, with a duration of 20 s, were made every 300 s. The sample cell was stirred with the flat tip of the syringe, rotating at 300 rpm. Bacitracin was titrated into the sample cell as a sequence of 28 injections. The time delay (to allow equilibration) between successive injections was 3 min. The heat of dilution of ion solutions (determined by injecting the divalent transition ion solution in the buffer-filled cell) was also measured. The measured dilution enthalpy of divalent transition ions was almost constant over the titrations.

Preparation of Bacterial Samples for Morphological Studies

S. aureus cells, cultured in nutrient-rich LB broth, were obtained from the prelogarithmic growth phase cultures. Samples were prepared according to Verbelen et al. (2006) and Meincken et al. (2005). Briefly, a 5.0-ml cell culture (1×10^6 CFU) was mixed with bacitracin (40 µg ml^{-1}), Zn(II) (20 µg ml^{-1}) or a bacitracin (40 µg ml^{-1})–Zn(II) (20 µg ml^{-1}) mixture; shaken well; and then left undisturbed for 3 h. The cell culture was then centrifuged down to a pellet and washed twice with Tris-HCl buffer (pH 7.0) to remove the excess compounds.

Imaging Cells

AFM measurements were performed in the air using the PicoScan System (Molecular Imaging, Tempe, AZ, USA). AFM tips (type II MAC tips, Molecular Imaging), coated with a magnetically conductive material, were employed with a lower spring constant range (1.2–5.5 N/m) than common tapping mode models. A topographical image and a phase image were obtained simultaneously in every single scan. Bacterial suspensions (10 µl) were dropped on a 2×2 cm^2 mica surface and then air-dried for AFM imaging.

To determine the effect of the antibiotic on the cell envelope and to ensure that the imaged damage was really due to the antibiotic, AFM imaging was done on both single-cell and multiple-cell samples. Analysis was also done with duplicate cultures for each antibiotic preparation.

TEM Experiments

Cell cultures for TEM were prepared by standard procedures for fixing and embedding biological samples (Bechtel and Bulla 1976; Beveridge et al. 1993). Samples were cut with a diamond knife into 50–60 nm thick slices, deposited on bare 200 mesh copper grids and stained with 2 wt% uranyl acetate followed by 2 wt% lead citrate, each for 5 min. Finally, grids with sections were washed twice with ultrapure water. Grids were dried overnight in a desiccator and examined using TEM (JEM-100CXII; JEOL, Tokyo, Japan) at 100 k*V* accelerating potential.

Results

Microcalorimetric Study of *S. aureus* Inhibition by Bacitracin

Typical thermogenic curves of *S. aureus* growing in a closed system are shown in Fig. 1. We observed the two typical peaks in the *P-t* curve, which may result from the

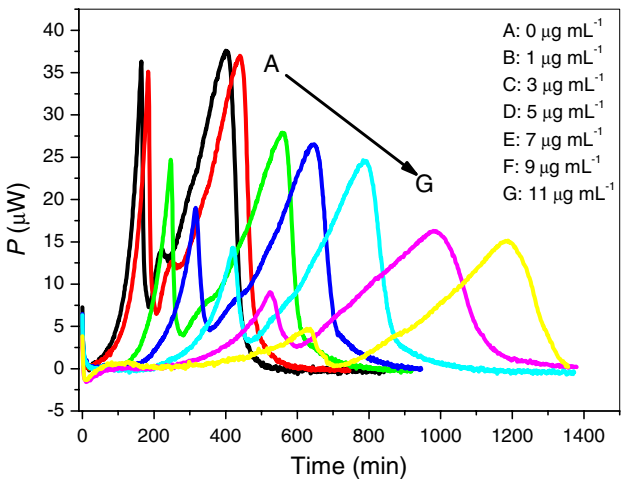

Fig. 1 Thermal curves of *S. aureus* growth induced by bacitracin. *A–G*, [bacitracin]: 0, 1, 3, 5, 7, 9, 11 µg ml^{-1}. The first peak of the growth rate constant (*k*) is shown in Table 1

two different metabolic "modes" of *S. aureus* (O'Neill et al. 2003; Zhu et al. 2006). The presence or absence of O_2 may be one of the important influences in the growth of bacteria, and it can influence the flux through different metabolic pathways. Under the conditions of the stop-flow microcalorimetric method, the reactor volume is only 0.6 ml and only the dissolved oxygen in the cell culture can be used by *S. aureus*. Initially, the aerobic metabolism of *S. aureus* dominates until the available oxygen is consumed; then, after a switch, a predominantly anaerobic metabolism occurs. This explains the observation of the typical peaks in the thermogenic curves (Fig. 1).

As described previously (Xie et al. 1988), the bacterial growth and heat generation in the logarithmic growth phase are exponential and can be calculated as follows:

$$P_t = P_0 \exp(kt) \quad (1)$$

or

$$\ln P_t = \ln P_0 + kt \quad (2)$$

where k represents the growth rate constant and P_0 and P_t are the bacterial growth of heat generation at the time $t = 0$ and $t = t$, respectively. The thermal curves of the logarithmic growth phase can be applied by Eqs. 1 and 2. Therefore, from the curve of $\ln P_t$ vs. t, we get the metabolic rate constant (k) of the bacteria induced by the different inhibitors, which can quantify the inhibitors' activity on the bacterial growth.

To describe the activity of bacitracin, its mixture with Zn(II) and Zn(II) on *S. aureus*, the inhibitory ratio (I/%) can be defined as follows:

$$I = \left[\frac{k_0 - k_c}{k_0}\right] \times 100\% \quad (3)$$

where k_0 is the growth rate constant of the control and k_c is the growth rate constant for *S. aureus* in the presence of an inhibitor with a concentration of C. Through the relationship of I vs. C, we get the half-inhibitory concentration (IC_{50}) for an inhibitor. The metabolic power–time curves of bacteria grown in the presence of bacitracin were obtained by microcalorimetric measurement, as shown in Fig. 1. From Fig. 1 we can see that the first maximal peak of heat power was decreased and the logarithmic growth phase of the time was increased when bacitracin increased (data shown in Table 1). According to this, we get the growth rate constant (k) of *S. aureus* induced by inhibitors. The growth rate constant (k), calculated from Eqs. 1 and 2, of the cultures treated with bacitracin decreased with increase bacitracin concentration and largely decreased with the additional Zn(II). However, the growth rate of *S. aureus* was stimulated by Zn(II) alone at low concentrations but inhibited at high concentration. The IC_{50} of bacitracin was calculated as 9.5 μg ml^{-1}, and the decreased to low values corresponded to the values with additional Zn(II) (Table 1). It has been reported that bacitracin requires the presence of divalent ions such as Zn(II), Mn(II), Cu(II), Ni(II) and Co(II) to increase its activity inhibited on bacteria (Stone and Strominger 1971).

In the fixed concentration of bacitracin at 3 μg ml^{-1}, the growth rate constant (k) of *S. aureus* markedly decreased in the presence of divalent metal ions, as shown in Fig. 2. Bacterial growth was not inhibited by metal ions at concentrations of 0–10 μg ml^{-1} (Zhao et al. 2000), which indicates that the activity of bacitracin on bacteria can be improved with the assistance of divalent metal ions. Mn(II) can largely decrease the growth rate constant (k) of *S. aureus* at low concentrations, but Cu(II), Ni(II), Co(II) and Zn(II) gradually inhibited *S. aureus* growth with increasing concentrations.

Kinetic Parameters of Bacitracin Interaction with Metal Ions by ITC

ITC is one of the most sensitive techniques that permit the direct measurement of thermodynamic changes in the course of binding between biomacromolecules and ligands

Table 1 Growth rate constant of *S. aureus* induced by bacitracin and Zn(II)

[Zn^{2+}] (μg ml^{-1})	[Bacitracin] (μg ml^{-1})							
	0	1	3	5	7	9	11	13
0	0.02847	0.02676	0.02239	0.02057	0.01736	0.01085	0.00937	0.00527
2	0.03022	0.02485	0.02201	0.01655	0.0138	0.00760	0.00530	
6	0.03197	0.02222	0.01403	0.00694	0.00605	0.00500		
10	0.03284	0.02295	0.01154	0.00660	0.00520			
20	0.03317	0.0215	0.01011	0.00500				
30	0.02907	0.01791	0.00730					
50	0.02643	0.01493						
70	0.02605	0.00995						
100	0.02584							

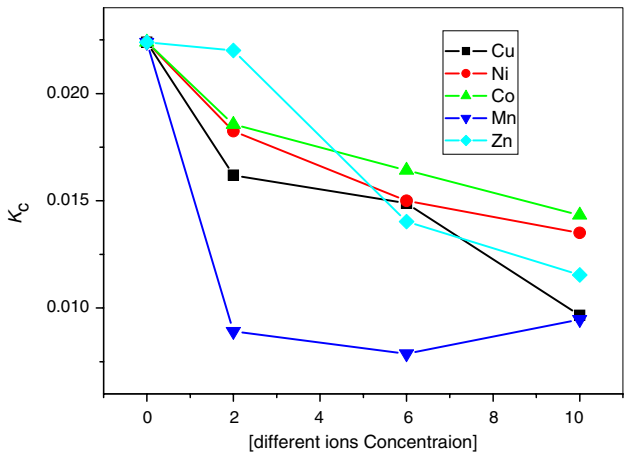

Fig. 2 Different divalent transition ions inhibited the growth rate constant (k) of *S. aureus*. Bacitracin concentration was fixed at 3 μg ml^{-1}

as well as kinetic aspects of complexation in biological systems. Since almost all chemical reactions involve heat change, ITC can be used for almost all chemical reaction systems, especially those that have no observable change by other probes during the reactions, such as protease and peptidase catalyst hydrolytic reactions, in which no obviously spectroscopic properties or pH changes occur. The binding model for a single set of sites was used to fit the incremental heat of the ith injection [ΔQ_i] of the total heat, Q_t, to the total titrant concentration, L_t, according to the following equations:

$$Q_t = nC_t\Delta H_b^0 V(1 + L_t/(nC_t) + 1/(nK_AC_t) - \{[1 + L_t/nC_t + 1/(nK_AC_t)]^2 - 4L_t/nC_t\}^{1/2})/2 \quad (4)$$

$$\Delta Q_i = Q_{(i)} + dV_i/\{2V[Q_{(i)} + Q_{(i-1)}]\} - Q_{(i-1)} \quad (5)$$

where dV_i is the volume of the titrant injected into the protein solution. The thermodynamic parameters ΔG_b and ΔS_b were calculated using the basic equation:

$$\Delta G_b^0 = -nRT \ln K_b = \Delta H_b - T\Delta S_b \quad (6)$$

where n is the number of binding sites of bacitracin, T is the experimental temperature and $R = 8.314$ J mol^{-1} K^{-1}. The observed enthalpy change (ΔH_{obsd}) includes the contribution from dilution of ions in the bacitracin solution and interactions between metal ions and bacitracin. Because the binding of bacitracin to divalent ions depends on the solution pH and proton release (Scogin et al. 1980), we chose the acetate buffer at pH 5.00 as the metal ion solution in order to observe metal–bacitracin complex precipitation (Seebauer et al. 1983).

A typical ITC profile for bacitracin binding to ions is shown in Fig. 3. A monotonic decrease in the heat evolved when amounts of bacitracin increased, which suggested that bacitracin displayed only one type of binding site. The binding isotherms were determined by fitting the data to the single set of sites binding model, which is consistent with the literature (Seebauer et al. 1983). The data for total heat released on each injection gave the best least squares fit to Eq. 4. The values of K_b, ΔH_b and n for all ions studied were obtained from Eqs. 5 and 6 and are given in Table 2. It is shown that the interaction between bacitracin and divalent metal ions is exothermic, and the precise order for metal binding affinity of divalent metal ions at pH 5.0 is Cu(II) ≥ Ni(II) > Co(II) > Zn(II) ≥ Mn(II), which is consistent with other established methods (Rao and Venkateswerlu 1989). Because the association constant of the manganese complex is too small to complete metal complexation at pH 5.0, a small amount of precipitate was observed at pH 7.1 (Scogin et al. 1980). From the ITC profile for Mn(II) at pH 5.0, there was a line indicating that the manganese was weakly bound to bacitracin. The kinetic parameters of bacitracin binding to Mn(II) can be neglected. The ITC profile for Cu(II) was different from that of other metal ions. When the molar ratio of bactracin to Cu(II) was 2, the heat changes of each titration drop suddenly increased, which indicated that the binding of Cu(II) was not simply to the glutamate carboxyl, the histidine imidazole and the thiazoline ring. There is a need for further study into the mechanism.

Features of AFM Imaging

As shown in Fig. 4a and b, AFM images revealed that the typical *S. aureus* had a relatively smooth surface without any ruptures or large pores, mean size of 1.20 × 0.85 μm (Fig. 2a), which was consistent with reports in the literature (Tollersrud et al. 2001). AFM images of *S. aureus* showed no damage to the bacterial cell surface (Fig. 4b) after cultures were treated by bacitracin at four times its IC_{50} (9.5 μg ml^{-1}) for 3 h. However, magnification of the bacterial surface shows an increase in roughness from that of the untreated cell. Some pore-like lesions with an average diameter of 60 nm were also observed in the treated samples compared with the pore-like lesions of untreated cells with 20 nm diameter (Fig. 5a, b. The circles in the Fig. 5 indicated that some pores was noticed on cell surface when treated by antibiotics.). *S. aureus* surface morphological changes, in the presence of the bacitracin–Zn(II) mixture, were also observed. As shown in Figs. 4c and 5c, the phenomenon of generated division gap was noticed on the extracellular cell wall; the inner changes of *S. aureus* can be seen by TEM. When the cell was treated with Zn(II) only, the surface were observed to be smoother (value of roughness) (Fig. 5d); this could be the metal ions interfering with the cell surface molecules.

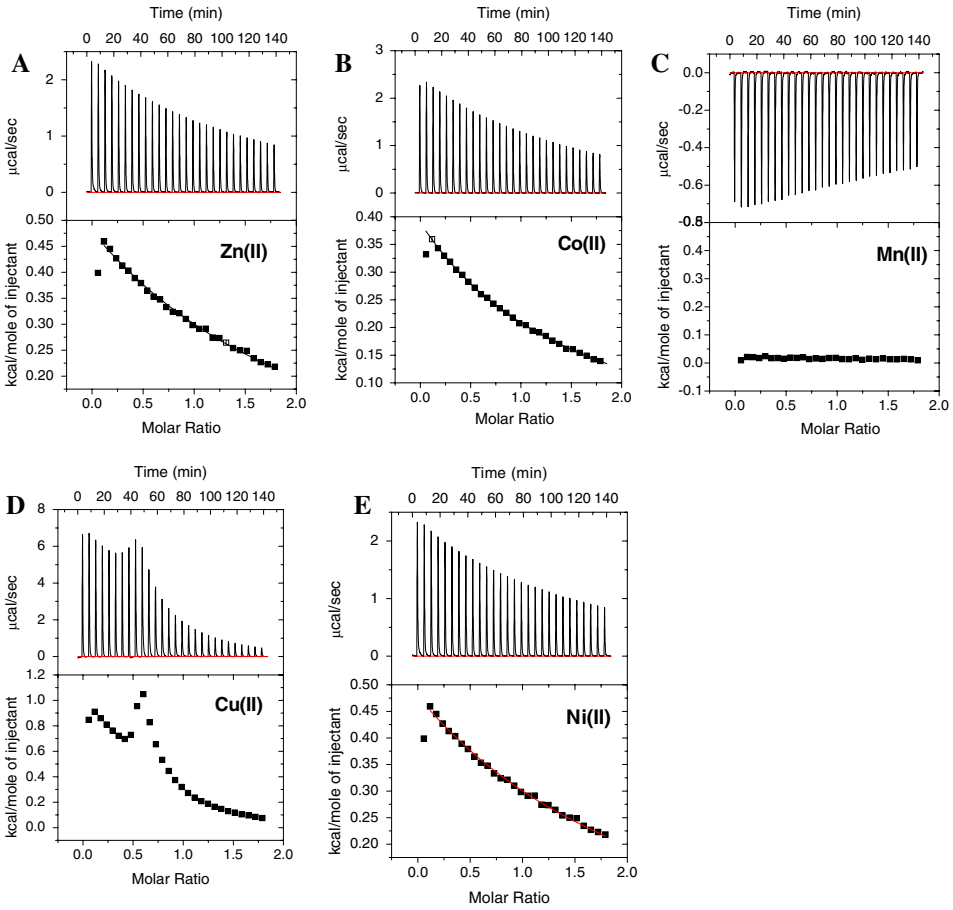

Fig. 3 Representative ITC data for bacitracin interaction with divalent metal ions. Raw data fitted to single-site model, obtained from injecting 10 µl of divalent metal ions solution (30 mM) into bacitracin solution (3 mM) in 10 mM acetic acid/sodium acetate buffer at 293 K are given at *top*, with a nonlinear least-squares fit of the heat released as a function of the ligand concentration (*solid squares*) at *bottom*. Thermodynamic parameters obtained for different mutants are given in Table 2

Table 2 Number of binding sites (n), binding constant (K_{ITC}), Gibbs energy (ΔG_{ITC}), enthalpy (ΔH_{ITC}) and entropy (ΔS_{ITC}) of the binding process of different metal ions with bacitracin in aqueous buffered solutions of pH 5.0 at 25°C

	Zn(II)	Co(II)	Cu(II)	Ni(II)
n	1.00 ± 0.1	1.08 ± 0.12904	1.009 ± 0.045	0.5790 ± 0.02641
K_{ITC} (M^{-1})	74.36 ± 2.432	214.0 ± 45.60	6,460 ± 2,698	1,381 ± 180.8
ΔG_{ITC}(kJ mol^{-1})	−2.556	−3.181	−5.200	−4.285
ΔH_{ITC}(kJ mol^{-1})	2.586 ± 0.060	0.807 ± 0.16	0.962 ± 0.058	0.970 ± 0.061
ΔS_{ITC} (J mol^{-1} K^{-1})	17.24	13.37	20.66	17.62

Thin Section of TEM

To gain further insight into the action of bacitracin on the *S. aureus* cell envelope, the effect of bacitracin and Zn(II) was investigated using thin-section TEM. Various stages of normal *S. aureus* cell morphology were observed by TEM. These images also were correlated well with the AFM images of *S. aureus* (compare Figs. 5 and 6). Selected images that represent the damage induced by bacitracin are shown in Fig. 4. Most notably, the treated cells show slightly thicker cell walls with characteristic dark, granular material concentrated in the center of the cells, believed to be chromosome (Matias and Beveridge 2006). From the microcalorimetric and AFM results, we hypothesize that bacitracin only inhibited cell wall biosynthesis but could not kill the bacteria. TEM imaging was, therefore, focused on the division events of *S. aureus*. At division sites, the staphylococcal wall forms in the middle of the cell, forming a septum (Fig. 6b).

When *S. aureus* was treated by bacitracin and bacitracin–Zn(II), most of the growing septum could not divide completely compared with the untreated cell (compare Figs. 7 and 8). The dark-stained septum of the bacteria treated by the bacitracin–Zn(II) mixture is more visible than that of cells treated by bacitracin only. Our results indicate that the daughter cells were unable to separate from each other, even

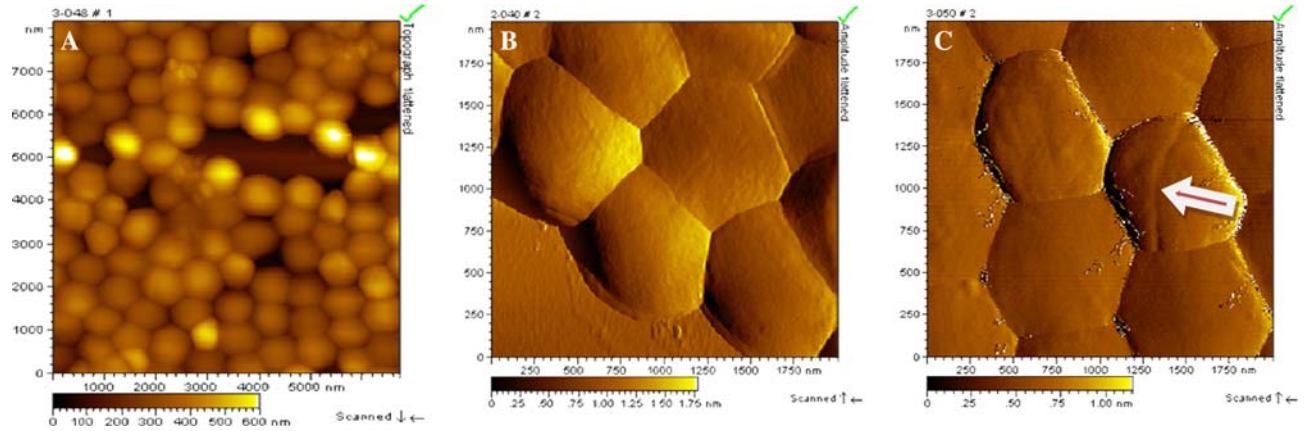

Fig. 4 Example of the common morphology of *S. aureus* without exposure to compounds; no structural or morphological changes appeared (**a**). Phase images of *S. aureus* exposure to bacitracin (**b**) or bacitracin–Zn(II) (**c**). The *S. aureus* surface was smooth in larger area in the phage image (**b**), but we can see the septal annulus on the central cell surface compared with the untreated cell (**c**)

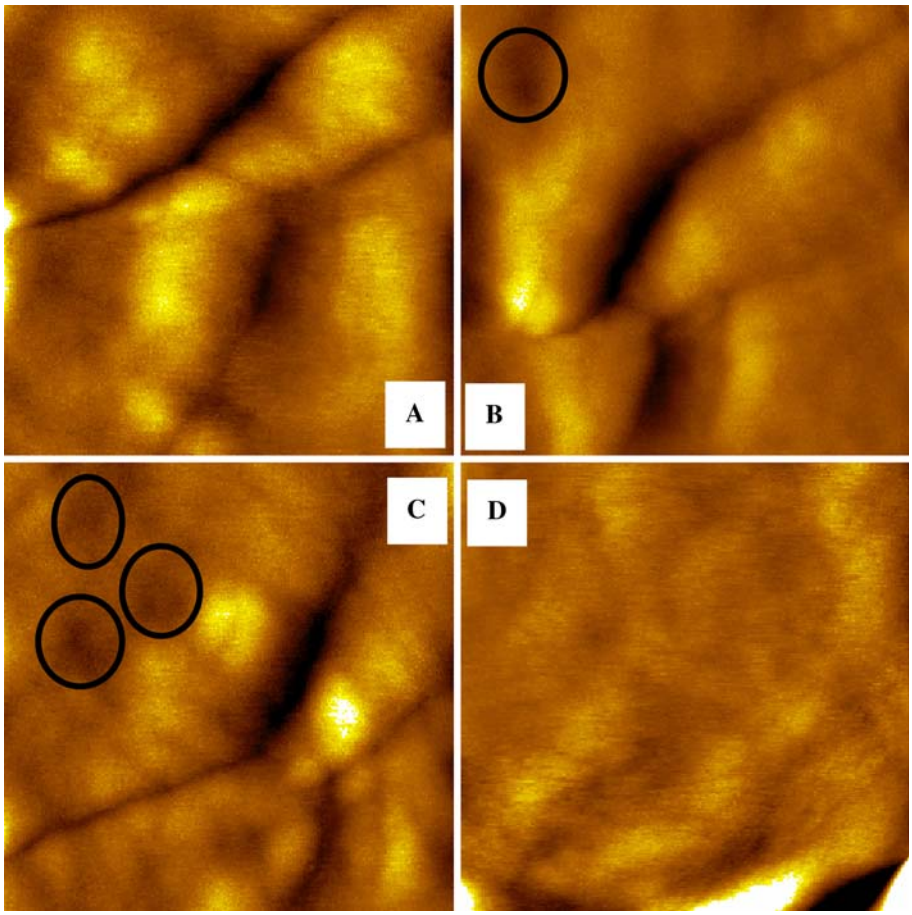

Fig. 5 High-magnification images of *S. aureus* surface ultrastructure (500 × 500 nm^2). **a** Native cells show normal division gap on the surface. **b** Although the gaps have been enlarged by bacitracin treatment (40 μg ml^{-1}), the surface shows some pores. **c** Activity of bacitracin was enhanced when the surface was treated with bacitracin (40 μg ml^{-1}) complexed with Zn(II) (20 μg ml^{-1}). **d** Cell surface treated with Zn(II) (20 μg ml^{-1}) became smooth

though the cell wall had formed (Fig. 7a, arrows). The visualized *S. aureus* cells maintained their coccus-shaped morphology in the presence of the bacitracin mixture and showed little evidence of damaged cell membranes. In the presence of Zn(II), the images of the bacteria were darker than those of bacteria in the absence of Zn(II) (Fig. 7b), probably due to adsorption of Zn(II) on the cell wall and uptake into the cell. Many daughter cells remained attached. Furthermore, it seemed that the cell walls were thicker than those of untreated cells.

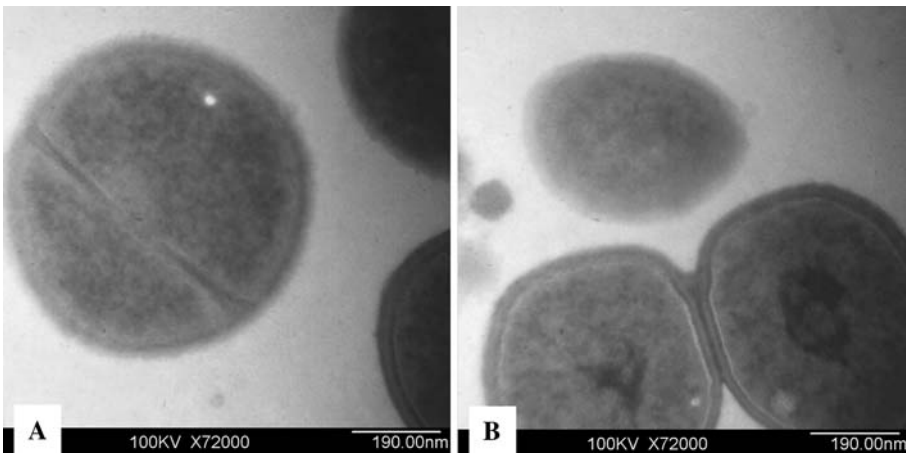

Fig. 6 Sequence of *S. aureus* division seen by thin-section TEM. **a** The septum has just been initiated and can be seen at the periphery of the cell wall. **b** Daughter cells are actively splitting away from one another so that only half of the septum remains intact

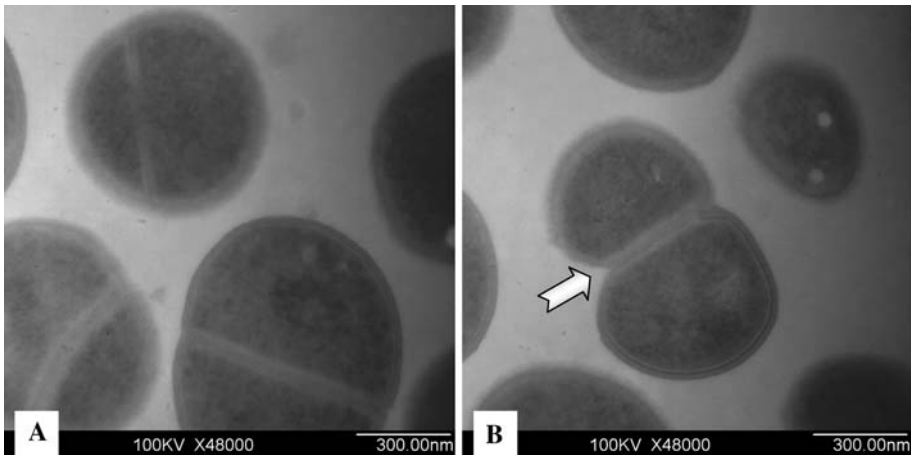

Fig. 7 Effect of bacitracin (40 μg ml^{-1}) on the growth and division of *S. aureus*.**a** The dark midline of highly reactive dense staining has been completed, but the upper peripheral wall of the septum has not appeared to split. **b** Advanced stage of septum splitting (*arrow*)

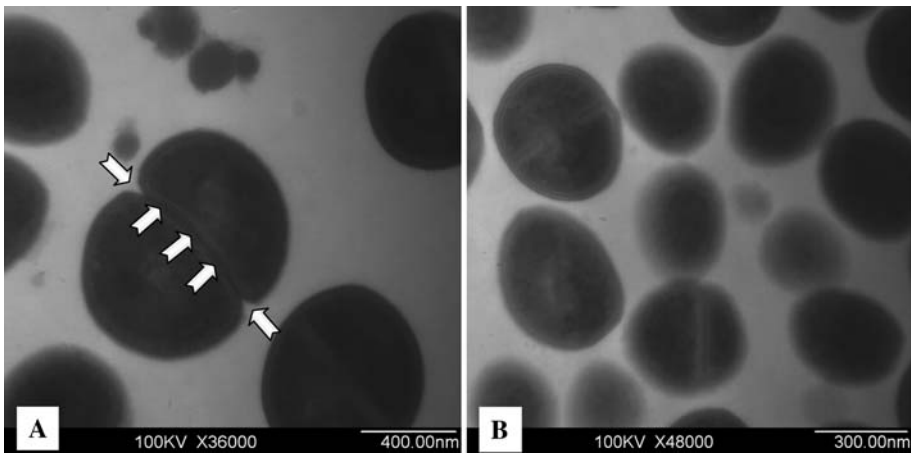

Fig. 8 Effect of bacitracin–Zn(II) complex (**a**) and Zn(II) (**b**) on the growth and division of *S. aureus*.**a** The cell periphery has been split and the cell wall formed, but the cells have not actually split away from each other (*Arrows* point to the dark midline region where the new cell wall has been completed.) **b** Cell wall thickness is increased, and many cells contact each other

Discussion

Because of the significance of the cell wall to bacterial survival, many experimental and theoretical studies have addressed the cell wall as a drug barrier. Drug-resistant gram-positive bacteria have already been identified as causing major public health problems (Lyon and Skurray 1987). It has been shown that bacitracin can inhibit cell wall biosynthesis in bacteria by forming a complex with IPP and divalent metal ions. Interaction between bacitracin and this functional phospholipid prevents the enzymatic dephosphorylation of the lipid, a step required in the biosynthesis of cell walls (Storm and Strominger 1967, 1973). More knowledge on the bacitracin influence on *S. aureus* morphology is therefore important for the development of analogous drugs.

We have observed the whole process of *S. aureus* growth in the absence and presence of bacitracin, the mixture bacitracin–Zn(II) and Zn(II). The growth rate constants were obtained based on Eqs. 1 and 2. The first and second peaks suggested that *S. aureus* adopts aerobic and anaerobic metabolism. The delayed time of the logarithmic phase indicated that cell growth and division were inhibited by bacitracin and the bacitracin–Zn(II) mixture, respectively. The growth rate constant of *S. aureus* decreased in the presence of bacitracin–Zn(II), which suggested that Zn(II) cooperated with bacitracin to reinforce the activity. However, the growth rate constant of *S. aureus* increased at low concentration and was inhibited at high concentration in the presence of Zn(II) only, which is consistent with the phenomenon of low-dose stimulation and high-dose inhibition, termed "hormesis" (the data are shown in Table 1 when bacitracin is absent) (Calabrese and Blain 2005). It was reported that bacitracin inhibited the main gram-positive bacteria with the divalent ions participating, such as Zn(II), Cu(II) and Mn(II) (Epperson and Ming 2000). The results suggested that Zn(II) may not coordinate with bacitracin but bind to the primary cell surface to assist bacitracin because of Zn(II) being inclined to coordinate with the NH_2 terminus outside the peptidoglycan layer.

The improving antimicrobial activity of bacitracin required transition metal ions in low concentration, and the growth rate constants of *S. aureus* decreased as the metal ion concentration increased. When the metal ion concentration was 10 μg ml^{-1}, the antimicrobial activity of bacitracin increased 30–56%. However, the activity of bacitracin–Mn(II) was largely improved compared with other metal ions. The biological activity of this antibiotic is not relative to the association constant of metal ion complexation. The association constant of Mn(II) complexes is too small to determine at pH 5.0, even at pH 7.1 (Garbutt et al. 1961), which indicates that the Mn(II) complexation with bacitracin is not necessary in the activity. On the other hand, metal ions can coordinate with cell wall molecules and increase the absorption of bacitracin on the cell surface. The ITC profile for binding to bacitracin is different from other metal ion binding processes. The main reason is that Cu(II) not only bound to the glutamate carboxyl, the histidine imidazole, the aspartate β-carboxyl and the thiazoline nitrogen but also influenced the three-dimensional conformation of bacitracin complexation.

To further elucidate the *S. aureus* cell wall ultrastructure affected by bacitracin, bacitracin–Zn(II) and Zn(II), we used high-resolution AFM and TEM to image the bacterial surface. In the presence of bacitracin (40 μg ml^{-1}), cell surfaces were obscured in AFM images. But the cell division just developed in the cytoplasm could be seen by TEM. Which revealed that bacitracin inhibited cell surface division. Some pores were noticed from AFM images in the presence of bacitracin–Zn(II) (bacitracin 40 μg ml^{-1}, Zn[II] 20 μg ml^{-1}), which may have been caused by either bacitracin aggregates or autolytic reactions (Matsuzaki et al. 1994; Wu et al. 1999). The pores on the outer membrane may in turn improve the uptake of bacitracin into the highly sensitive inner membrane (self-promoted uptake). As a result, cell division and growth were inhibited and the separation could not be completed. The cell autolysate, localized at the septum only, cannot function as normal, and the splitting system was settled on the "pseudomulticellular bacteria" (Giesbrecht et al. 1976). In *S. aureus*, cell autolysate can split the cross-wall into two leaflets (MacKenzie et al. 2002), each leaflet forming one hemisphere of the newly generated daughter cells (Fig. 5). The compact peptidoglycan networks of bacteria have their own cell wall hydrolases. In order to divide and separate, the cells must clear certain parts of their highly regulated walls (Giesbrecht et al. 1998). Cell division is preceded by the formation of a cross-wall at the centripetal cell region in staphylococci, which is invaginated into the plasma membrane and tightly apposed the peripheral wall in the cytoplasm. An important structural feature of the cross-wall is the splitting system. The splitting system is thought to be composed of periodically arranged tubular packets (i.e., murosomes) (Paul et al. 1995; Giesbrecht et al. 1997). When *S. aureus* was treated by the mixture of bacitracin with Zn(II), the noticeable ultrastructure of bacteria was an abnormally large splitting system within the thick cross-walls (Fig. 7a). The capacity of bacitracin to inhibit cell separation is probably based on its ability to reversibly deactivate all autolytic wall enzymes (i.e., murosomes) (Johansen and Gram 1996). The peptidoglycan layer is constructed from repeating disaccharide units of *N*-acetylglucosamine (GlcNAc) and peptidyl *N*-acetylmuramic acid (MurNAc) connected by b-1,4-glycosidic bonds. Since the hydrolysis of the long-chain undecaprenyl pyrophosphate into monophosphate is considered to be an essential step in peptidoglycan synthesis, the above observation suggests that bacitracin's binding to undecaprenyl pyrophosphate may interfere with cell wall hydrolysis (Hammes and Otto Kandler 1979; Podlesek et al. 2000). Furthermore, these murosome-associated wall autolysins have been identified as endo-b-*N*-acetylglucosaminidase and *N*-acetylmuramyl-L-alanine amidase (Yamada et al. 1996). As a result, bacitracin may affect the autolytic wall enzymes. Another interesting phenomenon from TEM images is that the different electron density of bacterial images suggests that Zn(II) is taken up by *S. aureus*. As we know, the NH_2-terminal domains are displayed on the cell surface and the COOH-terminal anchor structures are buried in the thick peptidoglycan layer (Schneewind et al. 1995; Pancholi and

Fischetti 1988). The main Zn(II) may coordinate with the cell surface, and parts of them are absorbed by cells. Thus, Zn(II) can not only stabilize the cell wall of macromolecules but also coordinate with the terminal peptides (Kotra et al. 1999), which have been used in the synthesis of nanoparticles (Zhou et al. 2007). When *S. aureus* was treated with Zn(II) at low concentration, the surface was smooth and cell numbers of the dividing states were increased, which is consistent with the microcalorimetric results.

In conclusion, we have investigated the antimicrobial activity of bacitracin and bacitracin–metal ions inhibited on *S. aureus* at 37°C. The affinity of metal ion binding to bacitracin was investigated by ITC, which is not relative with the antimicrobial activity of bacitracin–metal complexation. AFM and TEM revealed that the splitting system was largely delayed when *S. aureus* was treated with bacitracin or bacitracin–Zn(II). The antimicrobial activity of bacitracin only inhibited the growth and division initially from synthesis of the cell wall, especially the cell wall of the septal annulus. The increased activity of bacitracin with metal ions resulted from not only bacitracin being bound to metal ions but also the adsorption of bacitracin in the cell surface being bridged by divalent metal ions. The divalent metal ions provide assistance between bacitracin and the cell walls, while bacitracin inhibits the growth and division of *S. aureus*.

Acknowledgments We gratefully acknowledge the financial support of the National Natural Science Foundation of China (grants 30570015, 20621502, 20873096), the Research Foundation of the Chinese Ministry of Education ([2006]8-IRT0543) and the Natural Science Foundation of Hubei Province (2005ABC002).

References

Abdulrahim SMM, Haddadin SY, Odetallah NHM, Robinson RK (1999) Effect of *Lactobacillus acidophilus* and zinc bacitracin as dietary additives for broiler chickens. Br Poultry Sci 40:91–94

Bechtel DB, Bulla LA Jr (1976) Electron microscope study of sporulation and parasporal crystal formation in *Bacillus thuringiensis*. J Bacteriol 127:1472–1481

Beveridge TJ, Popkin TJ, Cole RM (1993) Electron microscopy. In: Gerhardted P (ed) Methods for general and molecular bacteriology. American Society for Microbiology, Washington DC, pp 42–71

Braga PC, Ricci D (1998) Atomic force microscopy: application to investigation of *Escherichia coli* morphology before and after exposure to cefodizime. Antimicrob Agents Chemother 42:18–22

Braga PC, Ricci D (2000) Detection of rokitamycin induced morphostructural alterations in *Helicobacter pylori* by atomic force microscopy. Chemotherapy 46:15–22

Braga PC, Ricci D (2002) Differences in the susceptibility of *Streptococcus pyogenes* to rokitamycin and erythromycin A revealed by morphostructural atomic force microscopy. J Antimicrob Chemother 50:457–460

Braga PC, Sasso M, Maci DS (1997) Cefodizime: effects of subinhibitory concentrations on adhesiveness and bacterial morphology of *Staphylococcus aureus* and *Escherichia coli*: comparison with cefotaxime and ceftriaxone. J Antimicrob Chemother 39:79–84

Calabrese EJ, Blain R (2005) The occurrence of hormetic dose responses in the toxicological literature, the hormesis database: an overview. Toxicol Appl Pharmacol 202:289–301

Chang TW, Gorbach SL, Bartlett JG, Saginur R (1980) Bacitracin treatment of antibiotic-associated colitis and diarrhea caused by *Clostridium difficile* toxin. Gastroenterology 78:1584–1586

Chaw KC, Manimaran M, Tay FEH (2005) Role of silver ions in destabilization of intermolecular adhesion forces measured by atomic force microscopy in *Staphylococcus epidermidis* biofilms. Antimicrob Agents Chemother 49:4853–4859

Dufrêne YF (2004a) Refining our perception of bacterial surfaces with the atomic force microscope. J Bacteriol 186:3283–3285

Dufrêne YF (2004b) Using nanotechniques to explore microbial surfaces. Nat Rev Microbiol 2:451–460

Epperson JD, Ming LJ (2000) Proton NMR studies of Co II complexes of the peptide antibiotic bacitracin and analogues: insight into structure–activity relationship. Biochemistry 39:4037–4045

Froyshov O (1984) The bacitracins: properties, biosynthesis, and fermentation. In: Vandamme EJ (ed) Biotechnology of industrial antibiotics. Marcel Dekker, New York, pp 665–694

Garbutt JT, Morehouse AL, Hanson AM (1961) Metal binding properties of bacitracins. J Agric Food Chem 9:285

Giesbrecht P, Wecke J, Reinicke B (1976) On the morphogenesis of the cell wall of staphylococci. Int Rev Cytol 44:225–318

Giesbrecht P, Kersten T, Maidhof H, Wecke J (1997) Two alternative mechanisms of cell separation in staphylococci: one lytic and one mechanical. Arch Microbiol 167:239–250

Giesbrecht P, Kersten T, Maidhof H, Wecke J (1998) Staphylococcal cell wall: morphogenesis and fatal variations in the presence of penicillin. Microbiol Mol Biol Rev 62:1371–1414

Hammes WP, Otto Kandler JW (1979) The sensitivity of the pseudomurein-containing genus *Methanobacterium* to inhibitors of murein synthesis. Arch Microbiol 123:275–279

Harel YM, Bailone A, Bibi E (1999) Resistance to bacitracin as modulated by an *Escherichia coli* homologue of the bacitracin ABC transporter BcrC subunit from *Bacillus licheniformis*. J Bacteriol 181:6176–6178

Hirotsu Y, Nishiuchi Y, Shiba T (1978) Total synthesis of bacitracin F. Peptide Chem 9:171–176

Johansen CTG, Gram L (1996) Changes in cell morphology of *Listeria monocytogenes* and *Shewanella putrefaciens* resulting from the action of protamine. Appl Environ Microbiol 62:1058–1064

Konigsberg W, Craig LC (1962) On bacitracin F. J Org Chem 27:934–938

Konz D, Klens A, Schörgendorfer K, Marahiel MA (1997) The bacitracin biosynthesis operon of *Bacillus licheniformis* ATCC 10716: molecular characterization of three multi-modular peptide synthetases. Chem Biol 4:927–937

Kotra LP, Golemi D, Amro NA, Liu GY, Mobashery S (1999) Dynamics of the lipopolysaccharide assembly on the surface of *Escherichia coli*. J Am Chem Soc 121:8707–8711

Lyon BR, Skurray R (1987) Antimicrobial resistance of *Staphylococcus aureus*: genetic basis. Microbiol Rev 51:88–134

MacKenzie FM, Greig P, Morrison D, Edwards G, Gould IM (2002) Identification and characterization of teicoplanin-intermediate *Staphylococcus aureus* blood culture isolates in NE Scotland. J Antimicrob Chemother 50:689–697

Matias VRF, Beveridge TJ (2006) Native cell wall organization shown by cryo-electron microscopy confirms the existence of a

periplasmic space in *Staphylococcus aureus*. J Bacteriol 188:1011–1021

Matsuzaki K, Murase O, Tokuda H, Funakoshi S, Fujii N, Miyajima K (1994) Orientational and aggregational states of magainin 2 in phospholipid bilayers. Biochemistry 33:3342–3349

Meincken M, Holroyd DL, Rautenbach M (2005) Atomic force microscopy study of the effect of antimicrobial peptides on the cell envelope of *Escherichia coli*. Antimicrob Agents Chemother 49:4085–4092

Ming LJ, Epperson JD (2002) Metal binding and structure–activity relationship of the metalloantibiotic peptide bacitracin. J Inorg Biochem 91:46–58

Monroe S, Polk R (2000) Antimicrobial use and bacterial resistance. Curr Opin Microbiol 3:496–501

Nagaraja TG, Chengappa MM (1998) Liver abscesses in feedlot cattle: a review. J Anim Sci 76:287–298

O'Neill NM, Vine GJ, Beezer AE, Bishop AH, Hadgraft J, Labetoulle C, Walker M, Bowler PG (2003) Antimicrobial properties of silver-containing wound dressings: a microcalorimetric study. Int J Pharm 263:61

Pancholi V, Fischetti VA (1988) Isolation and characterization of the cell-associated region of group a streptococcal M6 protein. J Bacteriol 170:2618–2624

Paul TR, Venter A, Blaszczak LC, Parr JRTR, Labischinski H, Beveridge TJ (1995) Localization of penicillin-binding proteins to the splitting system of *Staphylococcus aureus* septa by using a mercury-penicillin v derivative. J Bacteriol 177:3631–3640

Podlesek Z, Comino A, Herzog-Velikonja B, Zgur-Bertok D, Komel R, Grabnar M (1995) *Bacillus licheniformis* bacitracin resistance ABC transporter: relationship to mammalian multidrug resistance. Mol Microbiol 16:969–976

Podlesek Z, Comino A, Herzog-Velikonja B, Grabnar M (2000) The role of the bacitracin ABC transporter in bacitracin resistance and collateral detergent sensitivity. FEMS Microbiol Lett 188:103–106

Rao S, Venkateswerlu G (1989) Metal ion influence on the growth inhibition of *Neurospora crassa* by bacitracin. Microbiology 19:253–258

Rogers HJ, Perkins HR, Ward JB (1980) Microbial cell walls and membranes. Chapman and Hall, London

Schneewind O, Fowler A, Faull KF (1995) Structure of the cell wall anchor of surface proteins in *Staphylococcus aureus*. Science 268:103–106

Scogin DA, Mosberg HI, Storm DR, Gennis RB (1980) Binding of nickel and zinc ions to bacitracin A. Biochemistry 19:3348–3352

Seebauer EG, Duliba EP, Scogin DA, Gennis RB, Belford RL (1983) EPR evidence on the structure of the copper-bacitracin A complex. J Am Chem Soc 105:4926–4929

Sin DW, Ho C, Wong Y, Ho S, Ip AC (2005) Analysis of major components of residual bacitracin and colistin in food samples by liquid chromatography tandem mass spectrometry. Anal Chim Acta 535:23–31

Stone KJ, Strominger JL (1971) Mechanism of action of bacitracin: complexation with metal ion and C_{55} -isoprenyl pyrophosphate. Proc Natl Acad Sci USA 68:3223–3227

Storm DR (1974) Mechanism of bacitracin action: a specifc lipidpeptide interaction. Ann NY Acad Sci 235:387–398

Storm DR, Strominger JL (1967) Bacitracin: an inhibitor of the dephosphorylation of lipid pyrophosphate, an intermediate in the biosynthesis of the peptidoglycan of bacterial cell walls. Proc Natl Acad Sci USA 57:767–773

Storm DR, Strominger JL (1973) Complex formation between bacitracin peptides and isoprenyl pyrophosphates. J Biol Chem 248:3940–3945

Suurkuusk J, Wadso I (1982) A multichannel microcalorimetry system. Chem Sci 20:155–163

Tollersrud T, Berge T, Andersen RS, Lund A (2001) Imaging the surface of *Staphylococcus aureus* by atomic force microscopy. APMIS 109:541–545

Toscano WA Jr, Storm DR (1982) Bacitracin. Pharmacol Ther 16:199–210

Touhami A, Jericho MH, Boyd JM, Beveridge TJ (2006) Nanoscale characterization and determination of adhesion forces of *Pseudomonas aeruginosa* pili by using atomic force microscopy. J Bacteriol 188:370–377

Tsuji K, Robertson JH (1975) Improved high-performance liquid chromatographic method for polypeptide antibiotics and its application to study the effects of treatments to reduce microbial levels in bacitracin powder. J Chromatogr 112:663–672

Verbelen C, Dupres V, Menozzi FD, Raze D, Baulard AR, Hols P, Dufrêne YF (2006) Ethambutol induced alterations in *Mycobacterium bovis* BCG imaged by atomic force microscopy. FEMS Microbiol Lett 264:192–197

Wu M, Maier E, Benz R, Hancock REW (1999) Mechanism of interaction of different classes of cationic antimicrobial peptides with planar bilayers and with the cytoplasmic membrane of *Escherichia coli*. Biochemistry 38:7235–7242

Xie CL, Tang HK, Song ZH, Qu SS, Liao YT, Liu HS (1988) Microcalorimetry study of bacterial growth. Thermochim Acta 123:33–41

Yamada S, Sugai M, Komatsuzawa H, Nakashima S, Oshida T, Matsumoto A, Suginaka H (1996) An autolysin ring associated with cell separation of *Staphylococcus aureus*. J Bacteriol 178:1565–1571

Zhao R, Liu Y, Xie ZX, Shen P, Qu SS (2000) A microcalorimetric method for studying the biological effects of La^{3+} on *Escherichia coli*. J Biochem Biophys Methods 46:1–9

Zhou H, Fan T, Zhang XD, Guo Q, Ogawa H (2007) Novel bacteria-templated sonochemical route for the in situ one-step synthesis of ZnS hollow nanostructures. Chem Mater 19:2144–2146

Zhu JC, Liu Y, Wong WK, Zhou B, Yin J (2006) Investigation of antibacterial activity of two kinds of novel Schiff bases on *Escherichia coli* by microcalorimetry. Chin J Chem 24:1295–1300